Noise and spatial resolution characteristics of a clinical computed tomography scanner dedicated to the breast

Antonio Sarno, Giovanni Mettivier, Koen Michielsen, Juan José Pautasso, Ioannis Sechopoulos, et al.

Antonio Sarno, Giovanni Mettivier, Koen Michielsen, Juan José Pautasso, Ioannis Sechopoulos, Paolo Russo, "Noise and spatial resolution characteristics of a clinical computed tomography scanner dedicated to the breast," Proc. SPIE 12286, 16th International Workshop on Breast Imaging (IWBI2022), 1228619 (13 July 2022); doi: 10.1117/12.2624289

SPIE.

Event: Sixteenth International Workshop on Breast Imaging, 2022, Leuven, Belgium

Noise and spatial resolution characteristics of a clinical computed tomography scanner dedicated to the breast

Antonio Sarno[1,§,*], Giovanni Mettivier[1], Koen Michielsen[2], Juan José Pautasso[2], Ioannis Sechopoulos[2,3,4] and Paolo Russo[1]

[1]Università degli Studi di Napoli "Federico II" dep of Physics "E Pancini" & INFN Napoli, Naples, Italy
[2]Radboud University Medical Center, Department of Medical Imaging, Nijmegen, The Netherlands
[3]Technical Medical Centre, University of Twente, Enschede, The Netherlands
[4]Dutch Expert Center for Screening (LRCB), Nijmegen, The Netherlands
[§]presenter

*Corresponding author: sarno@na.infn.it

ABSTRACT

This work aims at evaluating the spatial resolution and noise in 3D images acquired with a clinical Computed Tomography scanner dedicated to the breast (BCT). The presampled modulation transfer function (MTF) and the noise power spectrum (NPS) are measured. In addition, the capability of the system in showing simulated lesions and microcalcification clusters was assessed via a phantom test. The impact of the selected reconstruction algorithm on MTF, NPS, and simulated lesion visibility was evaluated. The available algorithms are the Standard (Std) and Calcification (Calc) reconstructions, which use an isotropic reconstructed voxel edge of 0.273 mm and the high-resolution (HR) reconstruction algorithm that uses an isotropic reconstructed voxel edge of 0.190 mm. The spatial frequency (expressed in mm^{-1}) at which the MTF curve goes down to 10% ($MTF_{10\%}$) was found to be 1.0 mm^{-1} for the case of Std reconstruction in radial direction at the chest-wall; this value increases to 1.3 mm^{-1} and 1.5 mm^{-1} for the HR and Calc reconstructions, respectively. The distance from the isocenter did not impact the system spatial resolution. As expected, the improvement in the spatial resolution in the Calc and HR reconstruction algorithms is accompanied by an increase in the noise, especially at the higher frequencies, as shown in the 1D NPS. A phantom study showed that both simulated soft lesion with diameter of 1.8 mm and microcalcification cluster with grain diameter of 0.29 mm are visible, no matter what reconstruction algorithm is selected. Microcalcifications with diameter of 0.20 mm and 0.13 mm do not appear to be visible.

Keywords: CT dedicated to the breast, noise, spatial resolution, simulated lesion visibility

1. INTRODUCTION

This work aims at characterizing the clinical computed tomography scanner dedicated to the breast (BCT)[1] produced by Koning Health[2-5] in terms of spatial resolution, noise, and simulated lesion visibility. The spatial resolution is evaluated by means of the system modulation transfer function (MTF) and the noise characteristics via the analysis of the 3D and 1D noise power spectrum (NPS). A test phantom was used to evaluate the visibility of masses and simulated

16th International Workshop on Breast Imaging (IWBI2022), edited by Hilde Bosmans, Nicholas Marshall, Chantal Van Ongeval, Proc. of SPIE Vol. 12286, 1228619

microcalcifications. The intent of this work is to complete measurement data reported in Betancourt et al[4,5] by means of the evaluation of the MTF curves at varying positions in the scanner field of view. In addition, the MTF and NPS curves as well as the visibility of the simulated lesions were evaluated for the three reconstruction algorithms used by the clinical apparatus.

2. MATERIAL AND METHODS

2.1 The Koning Corp BCT scanner

Figure 1 shows a picture of the Koning Health BCT scanner installed at the Radboud UMC (Nijmegen, The Netherlands) and summarizes the scanner characteristics. The 300 image projections were acquired over the 360 deg scan angles with a detector frame rate of 30 Hz and with a pulsed x-ray source with pulse duration of 8 ms. The system permits to reconstruct a 3D image using either of three algorithms: Standard (Std), Calcification (Calc) and High Resolution (HR). The first two algorithms compute 3D images with isotropic voxel of 0.273 mm × 0.273 mm × 0.273 mm, while the HR algorithm reconstructs images with isotropic voxel of 0.190 mm × 0.190 mm × 0.190 mm.

Parameter	Value
Source-to-detector distance (mm)	923
Source-to-isocenter distance (mm)	650
N. of projections/360 deg scan	300
Anode/Filter combination	W/1.58 mm Al
Tube voltage (kV)	49
Tube current (mA)	12-200
Focal spot size (mm)	0.3
Spectrum HVL (mm Al)	1.39
Detector dimension (cm x cm)	40 × 30
Detector pixel pitch (mm)	0.338 (2 × 2 bin; native = 0.194)
Detector Scintillator (Material/thickness in mm)	CsI(Tl)/0.6 mm
Reconstructed voxel edge (mm, isotropic)	0.190 (HR); 0.273

Figure 1. Koning Corp BCT scanner installed at the Radboud UMC (Nijmegen, The Netherlands) and the table with specifications of the system on the right.

2.2 Modulation Transfer Function

The presampled point spread function (PSF) was evaluated by means of a 50 µm tungsten wire placed either parallel to the rotation axis, for the evaluation of the PSF in the radial (from the isocenter to the periphery of the field of view) and tangential (perpendicular to both axial direction and radial direction) directions or laying in the coronal plane, for the evaluation of the PSF in vertical direction (parallel to the axial direction)[6]. The wire was tilted of about 2 degrees for a proper presampled PSF evaluation. The MTF curves were obtained by applying the Fourier transform to the PSFs. The impact of the position on the evaluated MTF curve was assessed by placing the wire either at the scanner center of rotation or at the side of the field of view at 11 cm from the isocenter. In addition, the MTF was evaluated either at the chest wall side or at the nipple side at 13 cm from the chest.

2.3 Noise Power Spectrum

The 3D NPS was evaluated as suggested by Yang et al[7]. Briefly, the image of a 10-cm diameter cylinder made of PMMA was acquired two times and the difference image was computed in order to remove systematic noise components. The 3D Fourier transform was used for the computation of the 3D NPS from the noise image; 1D NPS was evaluated as the radial average from the central coronal slice of the 3D NPS.

2.4 Phantom study

To evaluate mass and microcalcification visibility, an image of a custom-made breast phantom (CIRS Inc, Norfolk, VA, USA)[8,9] were acquired at 50 mA. The used current was manually selected. The phantom consists of a background with attenuation coefficient equivalent to adipose breast tissue in addition to simulated spherical masses with diameter ranging between 1.80 mm and 6.32 mm made of epoxy resin, microcalcification $CaCO_3$ clusters with diameter of the grains ranging between 0.130 mm and 0.400 mm, and cylindrical fibers with the diameter ranging between 0.15 mm and 0.60 mm. The contrast to noise ratio (CNR) was evaluated in order to assess the mass visibility. It was defined as follows:

$$CNR = \frac{PV_M - PV_{bk}}{\sqrt{\frac{\sigma_M^2 + \sigma_{bk}^2}{2}}} \quad (1)$$

with PV_M and PV_{bk} average value of the pixels evaluated in region of interests (ROI) taken in the simulated mass and the test object background, respectively, and σ_M and σ_{bk} the corresponding standard deviations.

3. RESULTS

Figure 2 shows the tube output evaluated at the scanner isocenter for a full-scan rotation with a 6 cc ion chamber (model 20X6-6, RadCal Corp, Monrovia, CA USA) at varying tube currents. A linear fit of the tube output presented R^2 fitting parameter of 0.999.

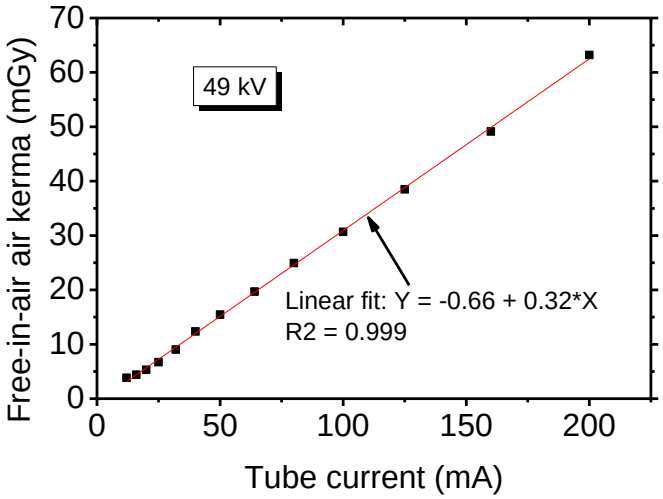

Figure 2. Tube output evaluated at the scanner isocenter for 360 deg scan.

The radial MTF curves are shown in fig. 3. The spatial frequency at which the MTF curve evaluated at the scanner isocenter for Std reconstruction goes down to 10% ($MTF_{10\%}$) is 1.0 mm^{-1}. It appears that x-ray pulses are sufficiently short (8 ms) such that the impact on spatial resolution when moving away from scanner isocenter is minimal (Std - side in fig. 3)[10]. $MTF_{10\%}$ increased to 1.3 mm^{-1} for HR reconstruction and to 1.5 mm^{-1} for Calc reconstruction. $MTF_{10\%}$ slightly reduces in tangential direction at 11 cm from the scanner isocenter. Hence this resulted 0.9 mm^{-1} for Std reconstruction and 1.2 mm^{-1} for both HR and Calc reconstructions (fig. 4).

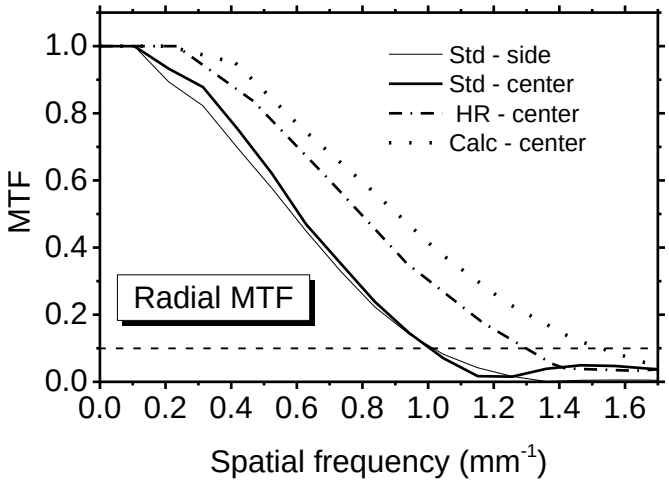

Figure 3. MTF evaluated in radial direction at the scanner isocenter for Std, Calc, and HR reconstruction and at 8 cm from the isocenter for Std reconstruction.

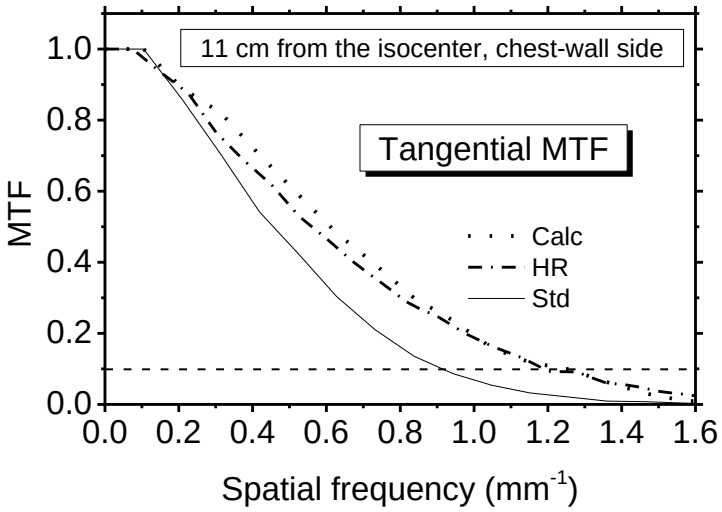

Figure 4. MTF evaluated in radial tangential direction at 11 cm from the isocenter for Std, Calc, and HR reconstruction at the chest-wall side.

Figure 5 reports MTF curves evaluated in vertical direction at the scanner isocenter. In these cases, $MTF_{10\%}$ ranges between 2.0 mm^{-1} evaluated for HR reconstruction and 2.3 mm^{-1} evaluated for Calc reconstruction. These MTF curves present an uptrend for low frequencies, exceeding the value at 0 mm^{-1}. This behavior is due by the shape of the presampled PSF, with conspicuous undershoots in vertical direction for evaluation at the chest wall side at the scanner isocenter (fig. 6a). Similar MTF shape was already shown for reconstruction kernels which determine similar undershot in PSF curves[11] or for phase contrast imaging[12]. These undershoots are not evident in the PSF evaluated in vertical direction at the nipple side at 13 cm from the chest (fig. 6b), this determining the absence of value higher than 1 in the corresponding MTF curve (fig. 7). In this position, the $MTF_{10\%}$ reduces to 2.0 mm^{-1} and 0.7 mm^{-1} in vertical and radial direction, respectively, these evaluated for Std reconstruction at the scanner isocenter.

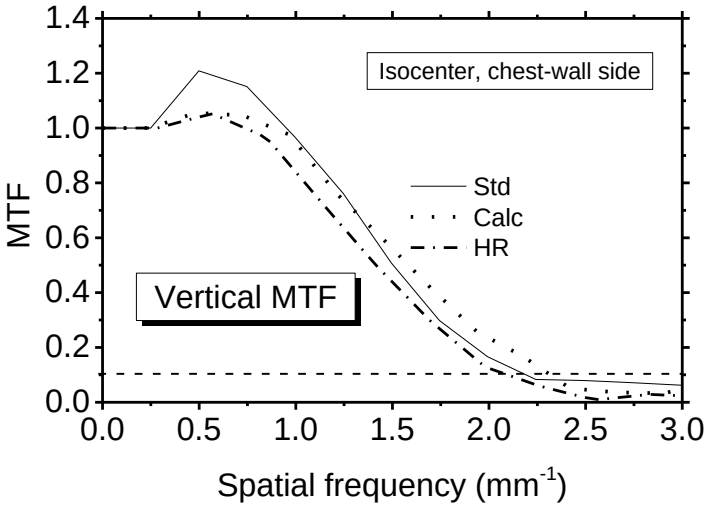

Figure 5. MTF evaluated in vertical direction at the scanner isocenter for Std, Calc, and HR reconstruction.

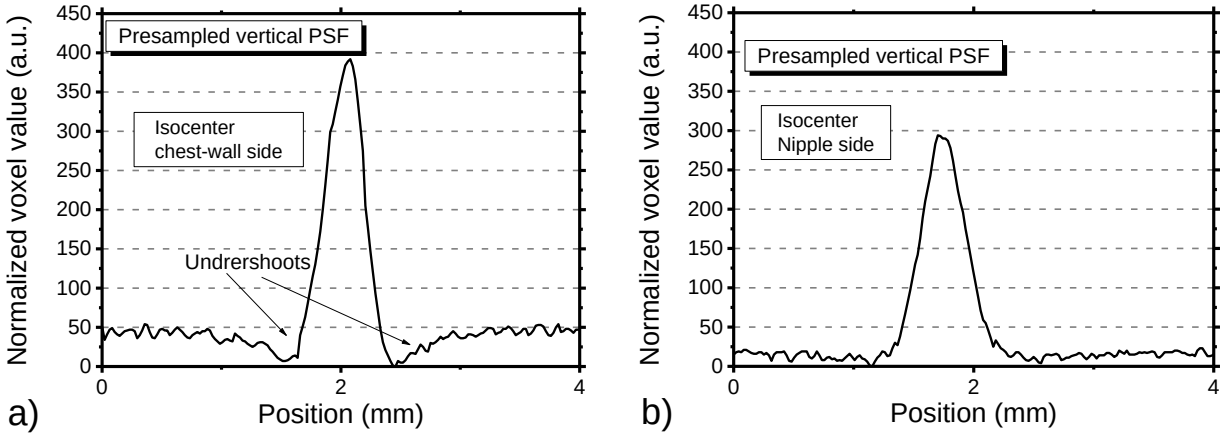

Figure 6. Presampled PSF in vertical direction at the scanner isocenter and at a) the chest-wall side and b) at the nipple side (13 cm from the chest-wall).

Figure 8a reports the 3D NPS, as shown in the three views in the 3D Fourier domain. Both in coronal and in sagittal views the silence cone is visible[7]. This is due to the field of view undersampling in the axial direction due to the cone beam nature of the acquisition[7]. The 1D NPS curves for the three available reconstruction algorithms are reported in fig. 8b. The improvement in the spatial resolution in the Calc and HR reconstructions is related to an increase in the noise power in the reconstructed images. Hence, the maximum value in the 1D NPS curves in these two cases is almost three times as high as that found for the Std reconstruction (fig. 8b). The use of a smaller pixel size in HR permits to avoid the aliasing present at the Nyquist frequency for the Calc reconstruction algorithm (fig. 8b).

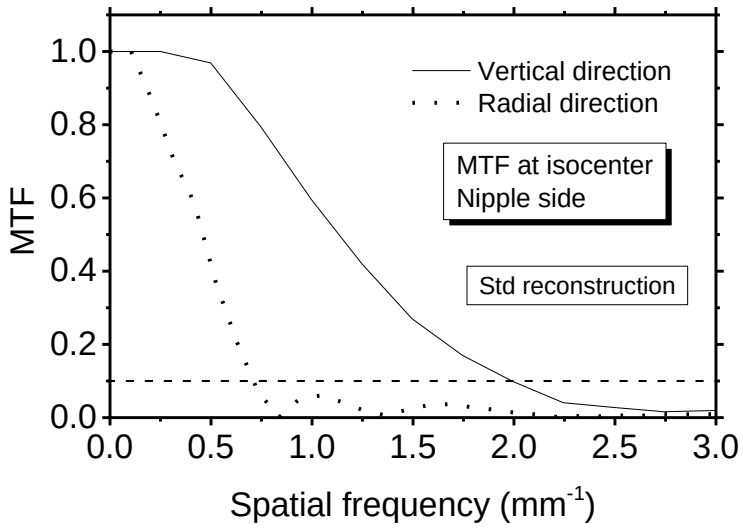

Figure 7. MTF evaluated in vertical and radial direction at the scanner isocenter and at nipple side (13 cm from the chest-wall) for Std reconstruction.

Confirming also the trend presented by a different BCT scanner setup[7], the 1D NPS curve reduces as the tube current increases (fig. 9a). Hence, it presents a peak of 860 HU^2mm^2 for 20 mA tube current, reducing to 110 HU^2mm^2 at 125 mA. For any current value, the peak of the 1D NPS curve is located at ~0.38 mm^{-1}. This reduction of the noise at the increasing of the current is also shown in fig. 9b. Here the standard deviation of pixel value is reported as function of the tube current. The pixel standard deviation was evaluated in 50 × 50 pixels ROI in axial slices (i.e. slices perpendicular to the rotation axis) at 1 cm from the chest wall. The resulting curve presents a monotonical trend from 38 HU evaluated for 20 mA down to 10 HU for 125 mA.

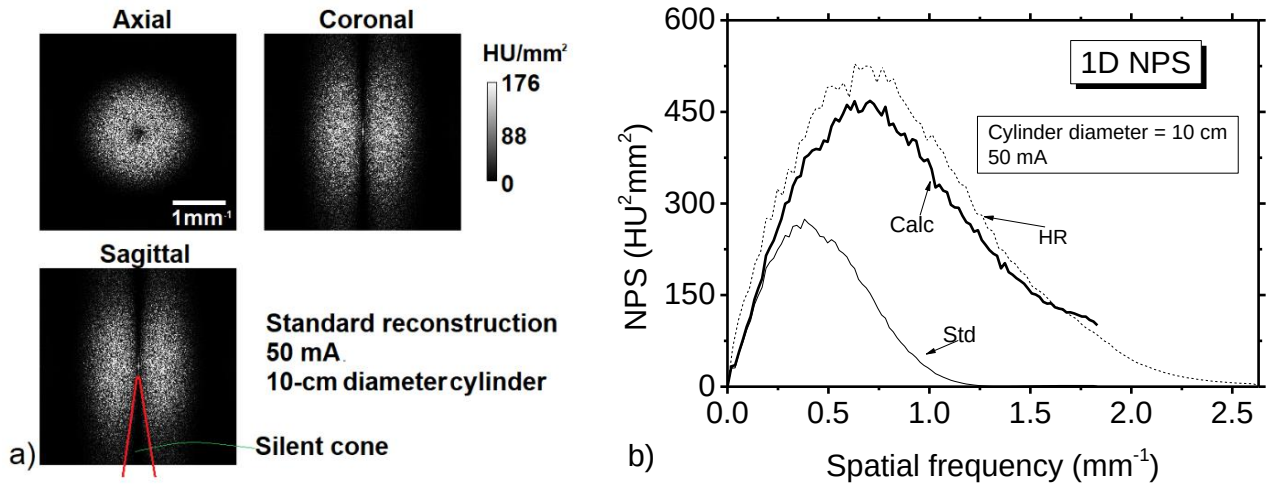

Figure 8. a) Axial, coronal, and sagittal views of the 3D NPS evaluated for PMMA cylindrical phantom with a diameter of 10 cm. In the sagittal view the silence cone due to the undersampling in z-direction can be seen. b) 1D NPS evaluated for PMMA cylinder with a diameter of 10 cm and 50 mA for Std, Calc, and HR reconstructions.

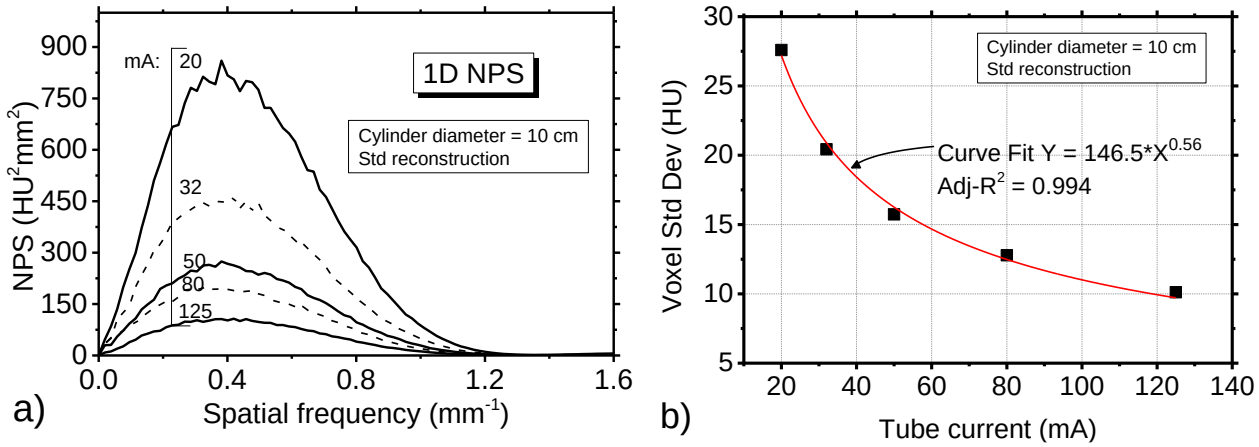

Figure 9. a) 1D NPS for tube current ranging between 25 mA and 125 mA. b) Voxel standard deviation evaluated at the scanner isocenter in axial slices of the 10-cm PMMA cylindrical phantom in 64 × 64 pixels region of interest; red line shows a non-linear power curve fit.

The conducted test phantom showed that the smallest simulated mass lesion, with a diameter of 1.8 mm, is visible for Std, Calc, and HR reconstructions (fig. 10). The CNR was evaluated for simulated lesion mass of 6.32 mm at 60 mm from the chest-wall both placed at 20 mm and 66 mm from the isocenter. In the axial slice containing the lesions, the CIRS phantom presented a diameter of 16 cm. CNR for the mass at 66 mm from the isocenter resulted 6.7, 2.2 and 2.1 for the Std, Calc and HR reconstructions, respectively. These values reduced to 3.4, 1.6 and 1.5 for the mass placed at 20 mm from the isocenter. The microcalcification cluster with 0.29 mm-diameter grains is visible for all three reconstruction algorithms (fig. 10). It is difficult to recognize microcalcification clusters with grains of 0.20 mm.

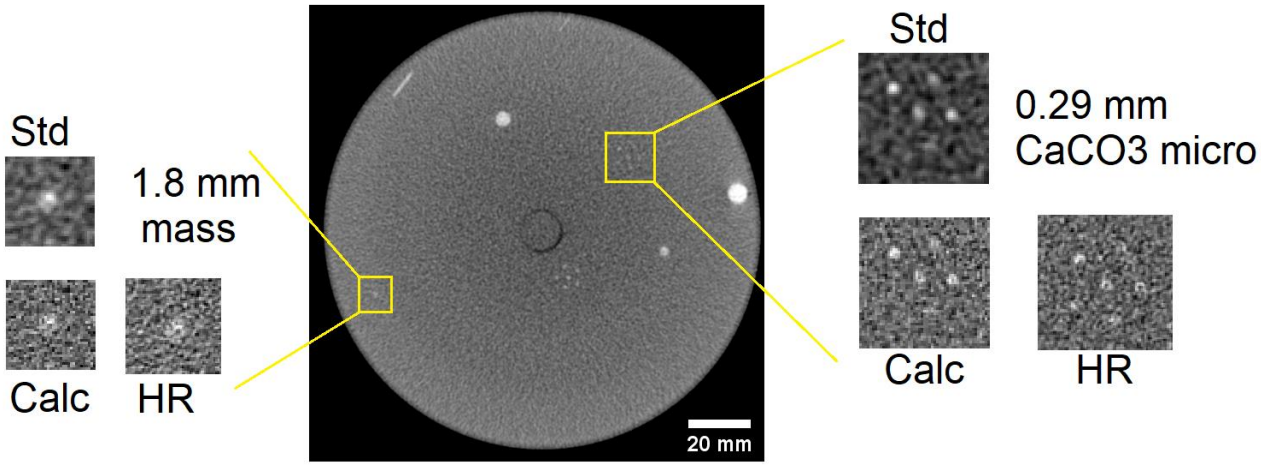

Figure 10. Breast phantom test. ROIs outline the 1.8 mm spherical mass of peroxin resin (left) and a microcalcification cluster with grain diameter of 0.29 mm for Std, Calc, and HR reconstructions. The large central image was obtained with a Std reconstruction by averaging 8 consecutives coronal slices. The scans were acquired at 50 mA. For each of the shown ROIs, window levels were selected to maximize the visibility of the inclusions.

4. CONCLUSIONS

In this work, we assessed the imaging characteristics of the Koning Health BCT scanner by evaluating the MTF, NPS, and a breast phantom. We focused on the impact of the three reconstruction algorithms used by the scanner unit. As expected, an increase in the $MTF_{10\%}$ was found for the special reconstruction algorithms aimed at increasing fine detail visibility (HR and Calc reconstructions). $MTF_{10\%}$ resulted 1 mm^{-1} for Std reconstruction at the chest wall side, increasing up to 1.5 mm^{-1} for Calc reconstruction; in the evaluations in Betacourt et al[5], this value resulted 1.7 mm^{-1} employing a voxel size of 100 µm. The distance from the isocenter did not show influences on the system spatial resolution. On the other hand, we observed a difference in the image CNR evaluated between a simulated lesion and the background signal, this resulted higher for phantom portion far from the scanner isocenter. The improvement of the spatial resolution due to Calc and HR reconstruction algorithms comes along with an increase of the noise power, as outlined by the evaluated 1D NPS curves. Microcalcification clusters with grain down to 0.29 mm resulted visible for all the investigated reconstruction algorithms; in Brombal et al[9], also the cluster with microcalcification grains of 0.20 mm was recognized.

ACKNOWLEDGMENTS

This work is in part supported by the Italian National Institute for Nuclear Physics (INFN) under the grant AGATA_GR5.

REFERENCES

[1] Sarno, A., Mettivier, G. and Russo P., “Dedicated breast computed tomography: basic aspects,” Med. Phys. 42, 2786-2804 (2015).
[2] website: http://koninghealth.com/ accessed on 11/01/2021
[3] Sechopoulos, I., Feng, S. S. J. and D'Orsi, C. J., “Dosimetric characterization of a dedicated breast computed tomography clinical prototype,” Med. Phys. 37, 4110-4120 (2010).
[4] Betancourt B. R., Ning, R., Conover, D. and Liu, S., “NPS Characterization and Evaluation of a Cone Beam CT Breast Imaging System,” J. X-ray Sci. Technol. 17(1), 17 – 40 (2009).
[5] Betancourt B. R., Ning, R., Conover, D. L. and Liu, S., “Composite modulation transfer function evaluation of a cone beam computed tomography breast imaging system,” Opt. Engineering 48, 117002 (2009).
[6] Sarno, A., Mettivier, G., Di Lillo, F., Cesarelli, M., Bifulco, P. and Russo, P., “Cone-beam micro computed tomography dedicated to the breast,” Med. Eng. Phys. 38, 1449-1457 (2016).

[7] Yang, K., Kwan, A. L., Huang, S. Y., Packard, N. J. and Boone, J. M., "Noise power properties of a cone-beam CT system for breast cancer detection," Med. Phys. 35, 5317-5327 (2008).
[8] Ramamurthy, S., D'Orsi, C. J. and Sechopoulos, I., "X-ray scatter correction method for dedicated breast computed tomography: improvements and initial patient testing," Phys. Med. Biol. 61, 1116 (2016).
[9] Brombal, L., Arfelli, F., Delogu, P., Donato, S., Mettivier, G., Michielsen, K. et al, "Image quality comparison between a phase-contrast synchrotron radiation breast CT and a clinical breast CT: a phantom based study," Sci Rep 9, 1-12 (2019).
[10] Gazi, P. M., Yang, K., Burkett Jr, G. W., Aminololama-Shakeri, S., Anthony Seibert, J. and Boone, J. M., "Evolution of spatial resolution in breast CT at UC Davis," Med. Phys. 42, 1973-1981 (2015).
[11] Boone JM, "Determination of the presampled MTF in computed tomography," Med Phys 28, 356-360 (2001).
[12] Sarno, A., Mettivier, G., Golosio, B., Oliva, P., Spandre, G., Di Lillo, F. et al, "Imaging performance of phase-contrast breast computed tomography with synchrotron radiation and a CdTe photon-counting detector," Phys. Med. 32, 681-690 (2016).